Theor Chim Acta (1992) 81: 223–235

Theoretica Chimica Acta

Ab initio studies of the low-lying states of BeO

Jun Irisawa and Suehiro Iwata

Department of Chemistry, Faculty of Science and Technology, Keio University, 3-14-1 Hiyoshi, Kohoku, Yokohama 223, Japan

Received February 27, 1991/Accepted March 23, 1991

Summary. *Ab initio* CI calculations are carried out for the ground and low-lying excited states of BeO. The potential energy curve (PEC), electronic dipole moment, dissociation energy, transition moment, and spectroscopic constants are evaluated. The configuration mixing plays a decisive role in determining the dipole moment of each state. The $A^1\Pi$ has a very small dipole moment near R_e. The evaluated vibrational spacings of the $X^1\Sigma$ and $A^1\Pi$ states are compared with the observed spectroscopic data. Based on the comparison, the dissociation energy of the ground state is estimated to be 4.3 ± 0.2 eV.

Key words: BeO – Potential energy curves – Dipole moment – Dissociation energy

1. Introduction

In recent years, chemiluminescence and laser fluorescence studies of alkali earth metal (Mg, Ca) oxidation reaction have been reported [1, 2]. But no such studies are found for Be. Because at the dissociation limit $Be(^1S) + O(^1D)$ and $Be(^3P) + O(^3P)$ lie closely to the ground state $Be(^1S) + O(^3P)$, it is expected that beryllium oxide (BeO) has many low-lying states. In the present paper we studied the electronic structure of low-lying states of BeO with *ab initio* CI calculations to stimulate the spectroscopic works for the singlet states as well as for the triplet states.

The alkali earth oxides have some specific features.

(i) The ground $X^1\Sigma^+$ lies close to the $a^3\Pi$ state.

(ii) The ground $X^1\Sigma^+$ state is correlated with the excited O atom (^1D) + the ground state metal (^1S) at the dissociation limit by the Wigner–Witmer rules.

(iii) The electronic structures of the low-lying states have strong dependence on the internuclear distance.

The previous theoretical calculations [3–12] for the alkali earth metal oxide indicate that most of low-lying states cannot be described by single reference SCF calculations. In particular, the electronic correlation has a decisive role in the electronic structure of the ground $X^1\Sigma^+$ state.

In both experimental and theoretical results [13–20], the dissociation energy D_e of the alkali earth oxides is correlated linearly with the equilibrium bond distance R_e. But BeO is exceptional; the reported D_e is not on an extrapolated line of the oxides of the other group 2 elements. Experimentally, the dissociation energy of BeO was estimated by the Birge–Sponer extrapolation of the vibrational level spacings [17], and mass spectrometry [18]. Their data are not well consistent with theoretical results [4, 9].

In this work, we studied the potential energy curves (PECs) of the several low-lying singlet and triplet states of BeO with the *ab initio* CI method. To examine the electronic structure of the states, we calculated the bond length dependence of the difference electron density contour map, the electronic dipole moment and transition dipole moments for $X^1\Sigma^+$, $A^1\Pi$, and $B^1\Sigma^+$. To estimate the dissociation energy, the vibrational energy levels for these states were calculated.

2. Theoretical method

In the previous works [21–23], we have found the importance of p type functions of Be as the electron-accepting orbitals. In a classical ionic bond picture, a beryllium atom in BeO is doubly charged. From our previous works, however, it is expected that the p type functions of Be accept the electrons and that they play an essential role in describing the bond. Therefore, in the present study, we augment the MIDI4 basis of Tatewaki and Huzinaga [24] with three p type CGTF's [25] and one d type GTFs; the basis set becomes [8s 5p 1d/4s 3p 1d]. For oxygen, MIDI4* [8s 4p 1d/4s 2p 1d] of Tatewaki and Huzinaga [24] was used. We also examine the role of the diffuse p-type function ($\alpha = 0.059$) on an oxygen atom, to describe a negatively charged oxygen.

To determine a set of the molecular orbitals for the POLCI calculations, first the closed shell self-consistent field (SCF) calculation is carried out for $(1\sigma)^2-(4\sigma)^2(1\pi)^4$, and then the valence type vacant orbitals (5σ), (6σ), and (2π) are determined by using Iwata's method [26]. Three orbitals (1σ), (2σ), and (3σ) which are originally from O 1s, Be 1s, and O 2s, respectively, are chosen as the core orbitals, and seven orbitals $(4\sigma)-(6\sigma)$, (1π), and (2π) which are composed of Be 2s, Be 2p, and O 2p, are chosen as active orbitals.

The reference configurations in the CI calculation for BeO are $[4\sigma, 1\pi, \{5\sigma, (6\sigma, 2\pi)^{0-1}\}^{0-4}]^6$, which stands for all possible configurations generated by filling six electrons in seven orbitals with two restrictions:

(1) a sum of the occupation number of $(6\sigma, 2\pi)$ is 0 to 1, and

(2) a sum of the occupation number of $(5\sigma, 6\sigma, 2\pi)$ is 0 to 4.

After releasing the restriction (1), the following types of the electron configurations from the reference configurations are generated: [core to active], [core to external], and [active to external], where the external orbitals comprise all of the virtual orbitals other than the valence type vacant orbitals.

In the C_{2v} symmetry, the configurations generated are [21; 4458] for $^1A_1$, [17; 4349] for $^1B_1$, [15; 4253] for $^1B_2$, [19; 6868] for $^3A_1$, and [20; 6843] for $^3B_1$, where the first number in [ ] is the number of the reference configuration state functions (CSF) and the second number is the number of the other CSF's taken into account.

For the *ab initio* CI calculations, the MOLYX system, which we have been developing in our laboratory, is used. To examine how the electronic structure changes, the dipole moment functions and the difference electron density maps are studied. A population analysis, recently proposed by Huzinaga et al. [27], is also carried out. The analysis produces the point charge distributed in the molecule, which can reproduce the same electric dipole moment as the one directly calculated with the wavefunction [27].

For the vibrational analysis on the potential energy curves, we use our program DIAVIB [28], which solves the Schrödinger equation of the nuclear motion numerically and is based on Cooley's method [29].

Most of computations were carried out on the SONY work stations NWS-830 and 841 in our laboratory, and some on HITAC M680 of the Institute for Molecular Science.

3. Results and discussion

3.1. The low-lying states and their character

Figures 1 and 2 show the calculated potential energy curves (PEC) for the singlet and triplet states, which are correlated with all of the states of $O(^3P) + Be(^1S)$ and $O(^1D) + Be(^1S)$ and with most of the states of $O(^3P) + Be(^3P)$. The dipole moment curves of CI wavefunctions for the low-lying three states and of the SCF wavefunction are given in Fig. 3. The enlarged potential energy curves for the low-lying states are given in Fig. 4. Table 1 shows the potential energy and transition dipole moment of three lowest singlet states and two triplet states.

The Hartree–Fock configuration (HFC) for $X^1\Sigma^+$ is $(1\sigma)^2(2\sigma)^2(3\sigma)^2(4\sigma)^2(1\pi)^4(5\sigma)^0(6\sigma)^0(2\pi)^0$; at near the equilibrium bond distance R_e, the $1\sigma_{1s}$, $3\sigma_{2s}$, $4\sigma_{2pz}$, and $1\pi_{2pxy}$ orbitals are localized on a O atom, while the orbital $2\sigma_{1s}$, $5\sigma_{2s}$, $6\sigma_{2pz}$, and $2\pi_{2pxy}$ are localized on a Be atom. To examine the character of the states, the difference electron density contour maps are shown in Figs. 5, 6 and

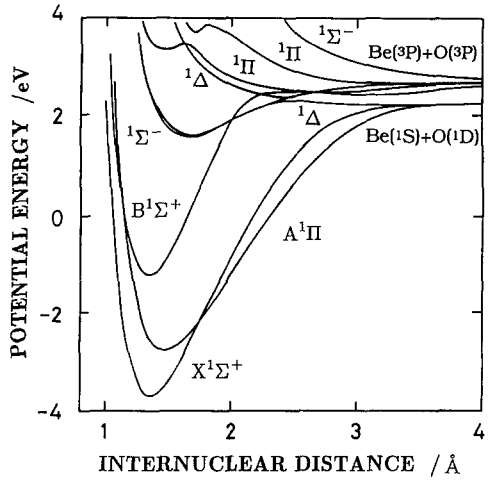

Fig. 1. The potential energy curves for the low-lying singlet states of BeO

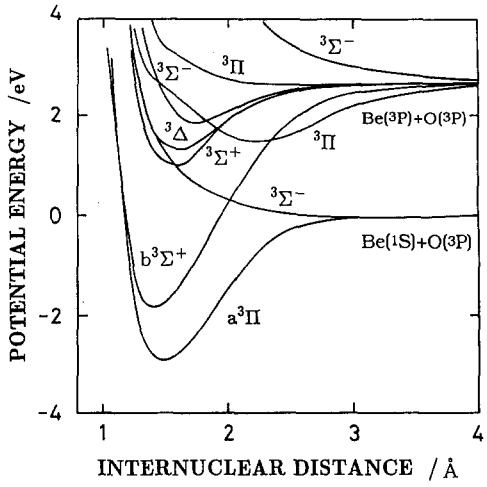

Fig. 2. The potential energy curves for the low-lying triplet states of BeO

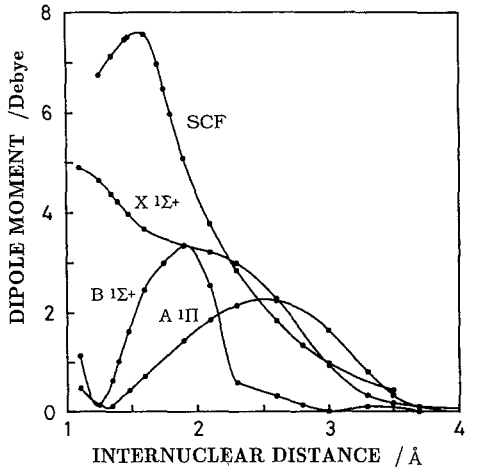

Fig. 3. The dipole moments for the low-lying singlet states of BeO as function of internuclear distance

7. The HFC has a strongly ionic character at most of the bond lengths as seen in Fig. 3. At large R the 4σ orbital changes from O $2pz$ to Be $2s$ atomic function, while the 5σ orbital changes from Be $2s$ to O $2pz$ atomic function. This switch of the character of the higher occupied orbitals affects the electronic structure and dipole moment of the low-lying states. The similar switch of the orbital character can be seen in 6σ and 7σ of MgO [30, 31].

The main configurations and the character of the lowest three singlet states are as follows:

(1) $X^1\Sigma^+$

At near R_e the HFC $4\sigma^2 1\pi^4$ is a dominant configuration, and two other configurations $4\sigma^1 1\pi^4 5\sigma^1$ and $4\sigma^1 1\pi^3 5\sigma^1 2\pi^1$ are mixed with the HFC. This mixing relaxes an extreme ionic character of HFC as can be seen from the dipole moment function in Fig. 3. The dipole moment of the CI wavefunction is substantially smaller than that of the SCF wavefunction. The difference electron

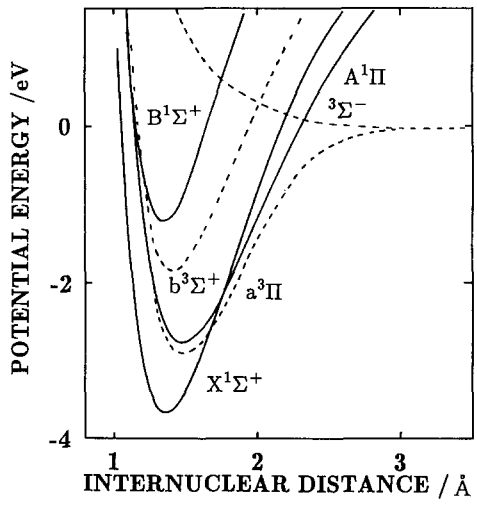

Fig. 4. The potential energy curves for the low-lying states of BeO

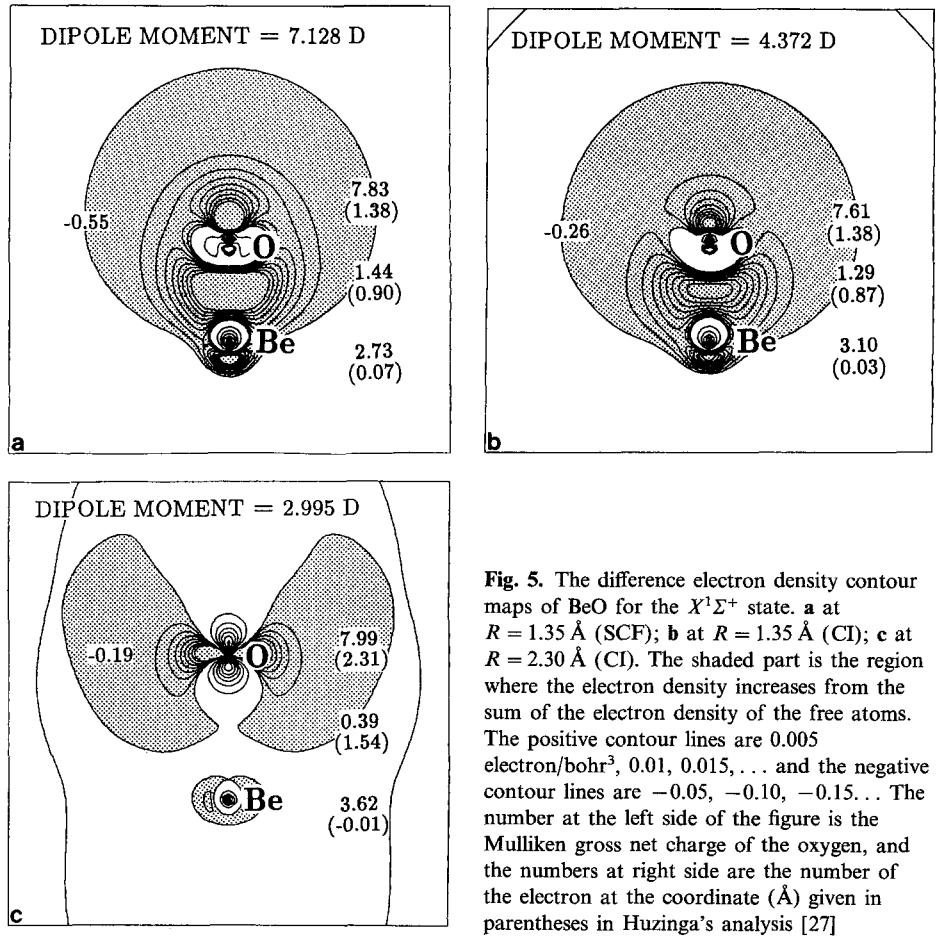

Fig. 5. The difference electron density contour maps of BeO for the $X^1\Sigma^+$ state. **a** at $R = 1.35$ Å (SCF); **b** at $R = 1.35$ Å (CI); **c** at $R = 2.30$ Å (CI). The shaded part is the region where the electron density increases from the sum of the electron density of the free atoms. The positive contour lines are 0.005 electron/bohr^3, 0.01, 0.015, ... and the negative contour lines are -0.05, -0.10, -0.15... The number at the left side of the figure is the Mulliken gross net charge of the oxygen, and the numbers at right side are the number of the electron at the coordinate (Å) given in parentheses in Huzinga's analysis [27]

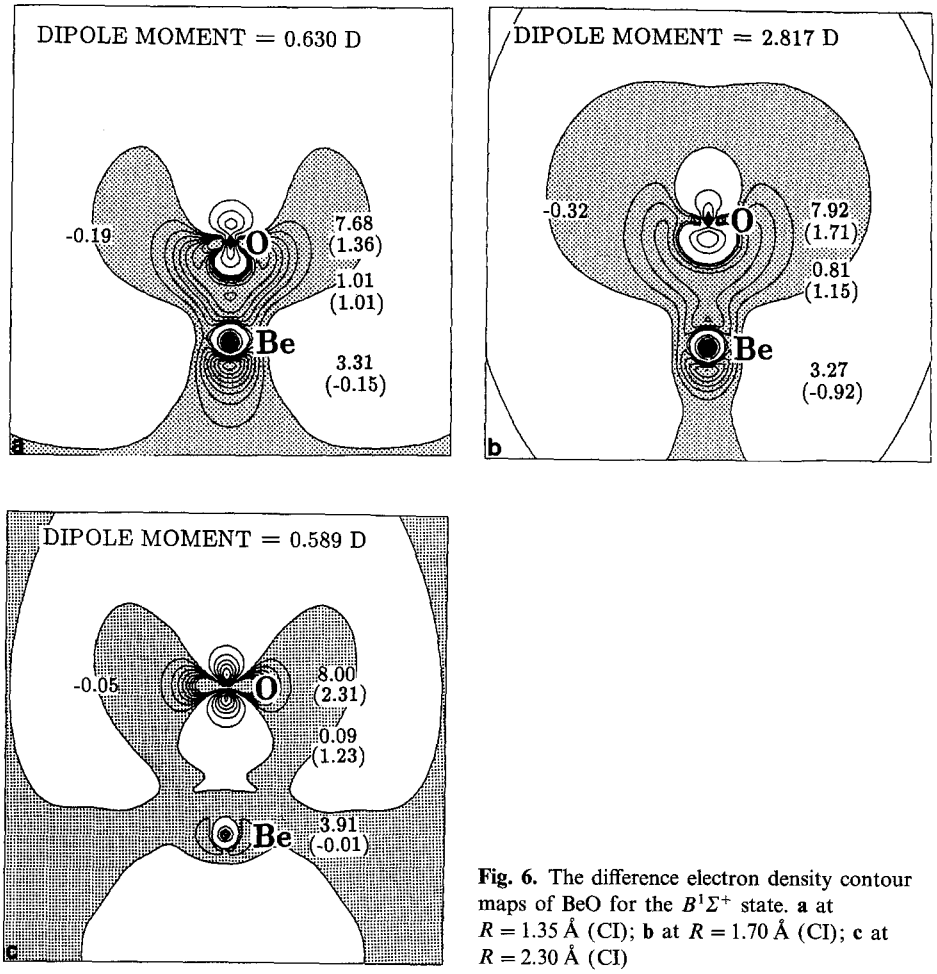

Fig. 6. The difference electron density contour maps of BeO for the $B^1\Sigma^+$ state. **a** at $R = 1.35$ Å (CI); **b** at $R = 1.70$ Å (CI); **c** at $R = 2.30$ Å (CI)

density contour maps at 1.35 Å in Figs. 5a and b show that the electron density is built up between two nuclei and that the convalent nature substantially increases in the CI wavefunction. Mulliken population analysis shows the gross charge on the oxygen atom is -0.547 for SCF and -0.258 for CI. Huzinaga's analysis given in the right side of the figures also demonstrates the increase of the electron density around Be in the CI wavefunction. Thus, BeO is not like $Be^{2+}O^{2-}$ but $Be^{x+}O^{x-}$ $(0.5 < x < 1)$. At the intermediate R the $4\sigma^0 1\pi^4 5\sigma^2$ configuration and at large R the $4\sigma^2 1\pi^2 5\sigma^2$ configuration are strongly mixed with the HFC. At the dissociation limit the $1^1\Sigma^+$ state becomes the excited atomic state of oxygen $O(^1D) + Be(^1S)$. The difference electron density contour map in Fig. 5c shows that the oxygen atom already becomes nearly $O(^1D)$ at 2.3 Å. The decrease of the dipole moment with an increasing R is determined mostly by the character change of the occupied orbital 4σ from O $2pz$ to Be $2s$.

(2) $B^1\Sigma^+$

The dominant configuration changes twice in this state while R is lengthened. Near the equilibrium bond distance $4\sigma^1 1\pi^4 5\sigma^1$ is a dominant configuration. The

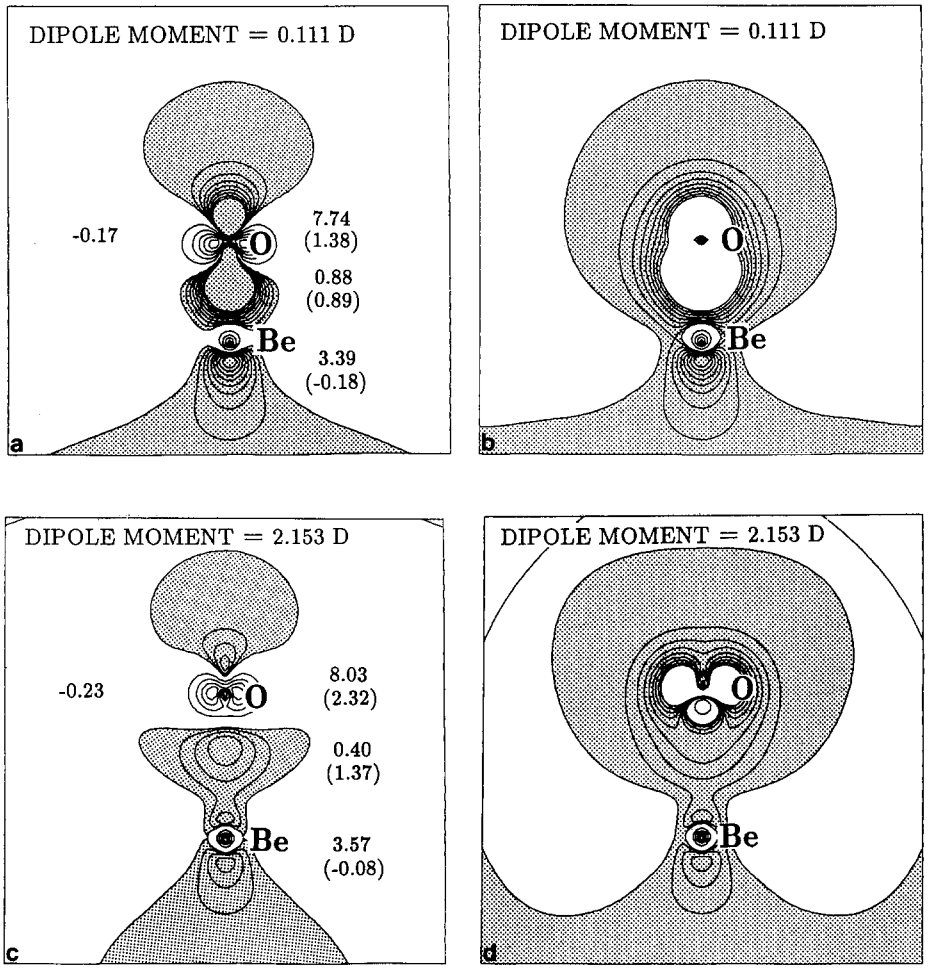

Fig. 7. The difference electron density contour maps of BeO for the $(\pi_x)^1(\pi_y)^2$ component of the $A^1\Pi$ state. **a** on the xz plane at $R = 1.35$ Å (CI); **b** on the yz plane at $R = 1.35$ Å (CI); **c** on the xz plane at $R = 2.30$ Å (CI); **d** on the yz plane at $R = 2.30$ Å (CI)

difference electron density contour maps are shown in Fig. 6a for $R = 1.35$ Å, Fig. 6b for $R = 1.7$ Å, and Fig. 6c for $R = 2.3$ Å. The dipole moment at R_e is very small, which results from the increase of electron density backward of Be, as can be seen from Fig. 6a. At the intermediate R, HFC is the second important configuration which results in a peak of the dipole moment function. This peak suggests that the ionic $(Be^+ + O^-)$ diabatic curve crosses near $R = 1.8$ Å with the diabatic curve which is correlated with $Be(^3P) + O(^3P)$.

At around 2.3 Å the main configuration becomes the HFC. This change indicates the avoided crossing. Because of this change, the PEC becomes flat, and the dipole moment function becomes small. In Huzinaga's analysis no charge between the nuclei is found. For longer than 3.0 Å the main configuration is the $4\sigma^1 1\pi^3 5\sigma^1 2\pi^1$ and thus the state dissociates to $Be(^3P) + O(^3P)$.

Table 1. Potential energy (eV)[a] and transition dipole matrix element (a.u.)

R (Å)	$X^1\Sigma^+$	$A^1\Pi$	$B^1\Sigma^+$	$\langle X\|z\|A\rangle$	$\langle X\|x\|B\rangle$	$\langle A\|x\|B\rangle$	$a^3\Pi$	$b^3\Sigma^+$
1.0	5.9179	9.2311	8.0197	0.6818	0.0964	0.0763	8.9817	7.9522
1.2	0.7254	2.6595	3.1212	0.7013	0.7952	0.0711	—	—
1.33	0.0000	1.2774	2.2622	0.6990	0.8750	0.2198	1.1283	1.9409
1.331[b]	0.0000[b]	1.3619[b]	2.6640[b]	0.6834[b]	0.8142[b]	0.2609[b]	—	—
1.4	0.0000	0.9851	2.5023	0.6847	0.9337	0.2878	0.8433	1.8278
1.5	0.2554	0.8915	2.8395	0.6560	0.7015	0.3887	0.7515	1.9243
1.7	1.1730	1.2874	3.9257	0.4851	0.9613	0.6238	1.1221	2.5708
1.9	2.2652	2.0537	2.2652	0.3909	0.6968	0.6993	1.8161	3.4307
2.0	2.7973	2.4637	5.5193	0.3494	0.5280	0.6882	2.1850	3.8798
2.3	4.1650	3.6338	6.1334	0.2305	0.0334	0.4014	3.0901	5.0204
2.8	5.4883	5.0702	5.4883	0.0088	0.0656	0.0214	3.5677	6.0047
3.3	5.8411	5.7537	6.2330	0.0093	0.1065	0.0441	3.6238	6.2246
3.5	5.8720	5.8456	6.2747	0.0088	0.6565	0.0213	3.6332	6.2689
7.0	5.9168	5.9266	6.3582	0.0003	0.0507	1.0596	3.6626	6.3582

[a] 0.0 eV is −89.46353 (hartree)
[b] Ref [10] full CI benchmark calculation. 0.0 eV is −89.59857 (hartree)

(3) $A^1\Pi$:
The main configuration is $4\sigma^2 1\pi^3 5\sigma^1$. If the orbital character of 4σ and 5σ changes smoothly with R, this single configuration is always the main configuration of the state. This is true in the present calculations, even though the orbitals are determined for the closed shell HFC. The $4\sigma^1 1\pi^3 5\sigma^2$ configuration at near R_e, and $4\sigma^1 1\pi^3 2\pi^2$ and $4\sigma^1 1\pi^3 6\sigma^2$ configurations at large R are mixed with the main configuration. Figures 7a and b are the difference electron density contour maps at $R = 1.35$ Å for the $(\pi_x)^1(\pi_y)^2$ component of the $^1\Pi$ state. The electron density increases in three parts: both ends and center of the molecule. Consequently, the dipole moment becomes very small. This is contrary to a simple picture that the state is of a nearly ionic nature of $Be^{+1}O^{-1}$. The dipole moment curve has a peak at 2.5 Å, which results from the similar reason with $B^1\Sigma^+$ state. Even at 2.3 Å, as shown in Figs. 7c and d, the electron density of the σ bonding region is still large, which is also seen in Huzinaga's analysis.

In MgO, the ionicity of the ground state has the similar picture $Mg^{\delta+}O^{\delta-}$ ($\delta = 2/3$) with BeO. The remarkable difference between two oxides exists in $B^1\Sigma^+$ state at near equilibrium bond distance. In BeO this state arises as a result of a single back charge-transfer excitation from the $X^1\Sigma^+$ state as the dipole moment indicates. On the other hand, in MgO the charge transfer from the $X^1\Sigma^+$ state almost does not occur as long as the dipole moment is noted [30, 31]. Generally, in the low-lying excited states of BeO the ionicity of the ground state is further relaxed, because the excitation is characterized by a back charge transfer from an oxygen orbital to a beryllium orbital.

3.2. Excitation energy and some spectroscopic constants

Table 2 shows the spectroscopic constants for the low-lying singlet and triplet states. The energy difference at the dissociation limit is given in Table 3. Since

Table 2. Spectroscopic constants of the low-lying electronic states of BeO

State	*Te* calc.	(eV) exp.	*Re* calc.	(Å) exp.	*ωe* calc.	(cm^{-1}) exp.
$^3\Sigma^-$	5.53		1.746		894.2	
$^1\Delta$	5.28		1.694		739.4	
$^1\Sigma^-$	5.25		1.679		740.2	
$^3\Delta$	5.03		1.634		841.4	
$^3\Sigma^+$	4.73		1.603		843.3	
$B^1\Sigma^+$	2.47	2.64	1.355	1.362	1515.8	1370.8
$b^3\Sigma^+$	1.85		1.416		1212.1	
	(1.93)[a]		(1.384)[a]		(1234)[a]	
$A^1\Pi$	0.91	1.17	1.479	1.463	1129.5	1144.2
			(1.456)[b]		(1167)[b]	
$a^3\Pi$	0.76		1.477		1091.9	
	(0.734)[a]		(1.463)[a]		(1270)[a]	
$X^1\Sigma^+$	0.00	0.00	1.369	1.331	1471.5	1487.3
			(1.313)[a]		(1629)[a]	

[a] See Ref. [6]
[b] See Ref. [9]

the basis set for O, which is optimized to $O(^3P)$, is not adequate for representing $O(^1D)$, the calculated energy of $Be(^1S) + O(^1D)$ is a little higher. Because of the error at the dissociation limit, the accuracy of the calculated adiabatic transition energy T_e is about 0.2 eV for the low-lying states.

Based on the calculated potential energy curves (PECs), we determined the vibrational levels by solving the Schrödinger equation numerically. The level spacings $G(v+1) - G(v)$ (the Birge–Sponer plot) are shown in Fig. 8, and they are compared with the experimentally-determined functions. The harmonic frequencies ω_e in Table 2 are evaluated by fitting the calculated vibrational energies to the Morse-potential energies.

The lowest three singlet states $X^1\Sigma^+$, $A^1\Pi$, and $B^1\Sigma^+$ are experimentally known. The calculated spectroscopic data for the $A^1\Pi$ state are in very good agreement with the experimental ones. This is understandable because this state can be approximately described by a single configuration for any bond length. Figure 8 demonstrates the agreement of the vibrational spacings up to the observed level $v = 25$. Therefore, the calculated PEC is expected to have high reliability over a large range of bond lengths. This suggests the possibility to use this PEC for determining the dissociation energy.

Table 3. Excitation energy at dissociation limit (eV)

State	Calc.	Exp.[a]
$Be(^3P) + O(^3P)$	2.69	2.72
$Be(^1S) + O(^1D)$	2.26	1.97
$Be(^1S) + O(^3P)$	0.00	0.00

[a] See Ref. [33]

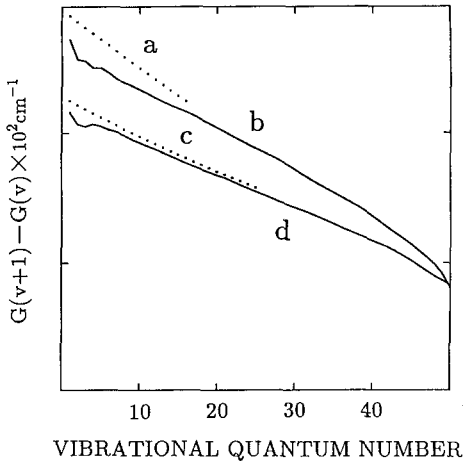

Fig. 8. The Birge–Sponer plots. *Line a*: The experimental plot for $X^1\Sigma^+$. *Line b*: The theoretical plot for $X^1\Sigma^+$. *Line c*: The experimental plot for $A^1\Pi$. *Line d*: The theoretical plot for $A^1\Pi$

Though the calculated R_e of the $X^1\Sigma^+$ state is longer by 0.037 Å than the experimental one, the harmonic frequency is in good agreement with the experimental one, and the Birge–Sponer plot in Fig. 8 also shows the overall agreement; the difference is at most 100 cm^{-1}. Experimentally, the vibrational levels of the $X^1\Sigma^+$ state are observed up to $v = 16$ [13]. Though this agreement might be fortuitous, the present calculation certainly may help to identify weak emission spectra from the upper states.

The vibrational levels of the $B^1\Sigma^+$ are observed only up to $v = 8$ [14]. As Fig. 1 shows, the potential energy curve of this state is very different from the Morse function, because of the state crossings. Although the calculated PEC of this state may not be so reliable as those of the other two lower singlet states, it is certain that the PEC is of non-Morse nature; thus the Birge–Sponer plot should be a higher order polynomial of the vibrational quantum number v than the quadratic.

The PECs and their calculated spectroscopic data of the two lowest triplet states $a^3\Pi$ and $b^3\Sigma^+$ are expected to be as accurate as those of the lowest two singlet states. Since the experimental determination of the vibrational spacing of the lowest triplet state $a^3\Pi$ is most desirable to determine the dissociation energy of BeO, as will be discussed below, we hope that our PECs and spectroscopic data of the triplet states help to find the T-T absorption or emission spectrum and the ro-vibronic perturbation among the singlet and triplet states.

In Table 1, the full CI results of Bauschlicher with the double zeta + polarization basis are inserted for comparison [10]. The present calculated transition dipole moments as well as vertical excitation energies are in very good agreement with the full CI results. This suggests that our CI calculations are adequate to determine the electronic structures of the states.

3.3. Dissociation energy

Many experimental efforts to determine the dissociation energy of alkaline-earth oxides have been reported [17–20]. However, there are uncertainties in the accurate determination. Therefore, Langhoff et al. proposed a method to estimate the dissociation energy of oxides of the group 1 and 2 elements [9].

(1) The past experiment

To determine the dissociation energy of BeO, two experimental results are reported; one is the spectroscopic [17] and the other is the thermochemical mass spectrometry [18]. Largerqvist et al. determined the dissociation energy $(D_0) = 3.9$ eV by extrapolation of $G(v)$ of $X^1\Sigma^+$, which was observed up to $v = 16$ [13]. By adding the zero point vibrational energy, they obtained $D_e = 4$ eV. Later, they succeeded in observing the vibrational levels of $A^1\Pi$ up to $v = 25$ [17]; the state has the same dissociation limit $Be(^1S) + O(^1D)$ with the ground state. By extrapolating the Birge–Sponer plot and adding the adiabatic energy difference T_e, they obtained $D_0 = 4.8$ eV and recommended this value rather than the previous value, because the higher vibrational levels are taken into account. On the other hand, Chupka et al. [18] determined $D_0 = 4.6$ eV by using mass spectroscopy to detect the high temperature vapor of BeO. To obtain the value, they considered the chemical equilibrium $BeO + O = Be + O_2$ in gas phase and assumed that equilibrium constant was approximated with ideal gas and the partial pressure P[O] = P[Be].

(2) The past *ab initio* calculations

Only a few papers [6, 11] reported the PEC of BeO near the dissociation limit. Schaefer [4] determined $D_e(X^1\Sigma^+) = 4.61$ eV by the NOCI calculation, using the experimental energy difference of $O(^1D)$ and $O(^3P)$ [33]. Langhoff et al. [9] carried out the SDCI calculations for a series of oxides of the group 1 and 2 elements with the extensive basis sets, but only near the equilibrium bond distance. To estimate the dissociation energy, they proposed the following procedure. For the oxides of Be, they used the calculated energy of $A^1\Pi$ at $R = R_e$, and assumed that the state $A^1\Pi$ is the ionic state $Be^+ + O^-$. The basic equation used is:

$$D_e^B = E(M^+) + E(O^-) - E(MO; R_e, A^1\Pi) - IP(M) + EA(O) + T_e(X^1\Sigma^+ - A^1\Pi), \quad (1)$$

where the experimental values are used for the ionization potential energy (IP) of the metal, the electron affinity (EA) of oxygen, and the adiabatic energy T_e. This formula can be rewritten as:

$$\begin{aligned} D_e^B &= \{[E(M^+) - E(M)] - IP(M)\} - \{[E(O) - E(O^-)] - EA(O)\} \\ &\quad + E(M) + E(O) - E(MO; R_e, A^1\Pi) + T_e(X^1\Sigma^+ - A^1\Pi) \\ &= \delta IP - \delta EA + D_e^{\text{calc}}(A^1\Pi) + Te(X^1\Sigma^+ - A^1\Pi), \end{aligned} \quad (1)'$$

where δIP and δEA are the calculated errors of the ionization energy and electron affinity, and D_e^{calc} is the calculated dissociation energy for the $A^1\Pi$ state. Thus, Eq. (1) merely makes correction of the error in the ionization energy and electron affinity of the atoms. Based on Eq. (1), they obtained $D_e = 4.69$ eV for BeO. But, the use of Eq. (1) for BeO, however, is not appropriate because, as mentioned above, the $A^1\Pi$ state of BeO near R_e is not the ionic state.

To further examine Eq. (1), we investigated the effect of the basis set of oxygen both on the electron affinity and on the dissociation energy $D_{eq}(A^1\Pi)$. The first basis set, MIDI4* described above, gives:

$$\delta IP = -0.09 \text{ eV} \quad \text{and} \quad \delta EA = -3.11 \text{ eV}.$$

With this basis set the direct *ab initio* dissociation energy is:

$$\begin{aligned} D_e^{\text{cal}} &= [E(Be\,^1S) + E(O\,^1D) - E(R_e\,^1\Pi)] \\ &\quad - [E(O\,^1D) - E(O\,^3P)] + [E(R_e\,^1\Pi) - E(R_e\,^1\Sigma^+)] \\ &= 4.932 - 2.266 + 0.907 = 3.57 \text{ eV}, \end{aligned} \tag{2}$$

On the other hand, Eq. (1) gives $D_e^B = 6.59$ eV, which is apparently overestimated because of the large error in the electron affinity of oxygen. If the experimental excitation energies for oxygen and BeO [32, 33] are used in the above Eq. (2), the dissociation energy is estimated as:

$$\begin{aligned} D_e^{\text{est}} &= [E(R = 7.0 \text{ Å}, {}^1\Pi) - E(R_e\,^1\Pi)] \\ &\quad - \Delta E(O\,^1D - {}^3P) + T_e \\ &= 5.03 - 1.97 + 1.17 = 4.22 \text{ eV}. \end{aligned}$$

In the second basis set, a diffuse p function ($\alpha = 0.059$) on oxygen is augmented. The electron affinity EA of oxygen is substantially improved though the error is still as large as $\delta EA(O) = -1.12$ eV. The EA of oxygen is improved by about 2 eV. Thus, Eq. (1) gives $D_{eq}^B = 4.58$ eV. However, the direct *ab initio* dissociation energy D_{eq}^{calc} does not change at all:

$$D_e^{\text{calc}} = 4.861 - 2.254 + 0.945 = 3.55 \text{ eV}$$

and

$$D_e^{\text{est}} = 4.97 - 1.97 + 1.17 = 4.17 \text{ eV}.$$

In other words, the substantial improvement of the calculated electron affinity does not much affect the PEC of the $A\,^1\Pi$ state, which clearly demonstrates the inappropriateness of use of Eq. (1) to estimate the dissociation energy of BeO. The present work is, however, not adequate to directly determine the accurate absolute value. The present PEC near equilibrium bond distance reproduces the experimental spectroscopic constants well, as can be seen in Fig. 8 and Table 2. The sum of the errors in the calculated and experimental vibrational energies up to $v = 25$ is only 0.08 eV. Therefore, by using $D_{eq}^{\text{est}} = 4.2$ eV plus the error of vibrational spacing, our recommended value becomes $D_e = 4.3 \pm 0.2$ eV.

4. Conclusions

The potential energy curves of the low-lying states of BeO are obtained by *ab initio* CI calculations. The electronic dipole moment, transition moment, spectroscopic constants, and dissociation energy are evaluated. The following conclusions are drawn:

(1) The low-lying states of BeO interact with the ionic diabatic curve. Therefore, the configuration mixing plays an important role in determining the electronic structure and dipole moment.

(2) The ground $X\,^1\Sigma^+$ state is not like $Be^{2+}O^{2-}$ but like $Be^{x+}O^{x-}$ $(0.5 < x < 1)$.

(3) The $A\,^1\Pi$ and $B\,^1\Sigma^+$ states near R_e are a single back charge-transfer excitation from oxygen to beryllium.

(4) The evaluated vibrational spacings of the $X^1\Sigma^+$ and $A^1\Pi$ states are in good agreement with the observed data. The dissociation energy of the ground state is estimated to be 4.3 ± 0.2 eV.

(5) We expect that our spectroscopic constants for the triplet states help the future spectroscopic studies.

(6) Huzinaga's population analysis is useful in studying the electronic structure, particularly when the difference electron density contour map is simultaneously used.

Acknowledgement. A part of the present work is supported by a Grant-in-Aid for Scientific Research for Priority Area by the Ministry of Education, Science and Culture, Japan (No.63606514 and No. 01606001).

References

1. Cox JW, Dagdian PJ (1984) J Phys Chem 88:2455
2. Irvin JA, Dagdian PJ (1980) J Chem Phys 73:176
3. Huo WM, Freed KF, Klemperer W (1967) J Chem Phys 46:3556
4. Schaefer HF (1971) J Chem Phys 55:176
5. O'Neil SV, Pearson PK, Schaefer HF (1971) Chem Phys Lett 10:404
6. Pearson PK, O'Neil SV, Schaefer HF (1972) J Chem Phys 56:3938
7. Bauschlicher CW, Yarkony DR (1980) J Chem Phys 72:1138
8. Partridge H, Bauschlicher CW, Langhoff SR (1984) Chem Phys Lett 31:446
9. Langhoff SR, Bauschlicher CW, Partridge H (1986) J Chem Phys 84:4474
10. Bauschlicher CW, Langhoff SR (1988) Theor Chim Acta 73:43
11. Witko M, Bonacic-Koutecky V (1986) Int J Quan Chim 29:1535
12. Bauschlicher CW, Langhoff SR (1986) Supercomputer simulations in chemistry. In: Dupuis M (ed) Lecture notes in chemistry, Vol 44. Springer-Verlag, Berlin Heidelberg New York London Paris Tokyo, p 75
13. Largerqvist A, Westoo R (1945) Arkiv Mat Ast Fysik 31A:No 21
14. Largerqvist A, Westoo R (1945) Arkiv Mat Ast Fysik 32A:No 10
15. Largerqvist A (1946) Arkiv Mat Ast Fysik 33A:No 8
16. Largerqvist A (1947) Arkiv Mat Ast Fysik 34B:No 23
17. Largerqvist A (1954) Arkiv Fysik 7:473
18. Chupka CF, Berkowitz J, Giese CF (1959) J Chem Phys 30:827
19. Srivastava RD (1976) High Temp Sci 8:225
20. Shofield K (1967) Chem Rev 67:707
21. Hashimoto K, Yoda N, Iwata S (1987) Chem Phys 116:193
22. Hashimoto K, Osamura Y, Iwata S (1987) J Mol Struct (Theochem) 152:101
23. Hashimoto K, Iwata S (1989) J Phys Chem 93:2165
24. Tatewaki H, Huzinaga S (1980) J Comp Chem 1:205
25. Dunning TH, Hay PJ (1977) Method of electronic structure theory. In: Schaefer HF (ed) Modern theoretical chemistry, Vol 3. Plenum, New York London, p 1
26. Iwata S (1981) Chem Phys Lett 83:134
27. Huzinaga S, Sakai Y, Miyoshi E, Narita S (1990) J Chem Phys 93:3319
28. Sato S, Iwata S (1983) J Chem Phys 79:4805
29. Cooley JW (1961) Math Compt 15:363
30. Thummel H, Klotz R, Peyerimhoff SD (1989) Chem Phys 129:417
31. Thummel H, Klotz R, Peyerimhoff SD (1989) Chem Phys 135:229
32. Huber KP, Herzberg G (1979) Molecular spectra and molecular structure, Constants of diatomic molecules. Van Nostrand Reinhold, New York
33. Radzig AA, Smirnov BM (1985) Reference data on atoms, molecules and ions. In: Toennies JP (ed) Springer series in chemical physics, Vol 31. Springer, Berlin Heidelberg New York Tokyo